Compartmentalized Cell Envelope Biosynthesis in *Mycobacterium tuberculosis*

Julia Puffal[a,1], Ian L. Sparks[a,1], James R. Brenner[a], Xuni Li[b,c], John D. Leszyk[b,c], Jennifer M. Hayashi[a], Scott A. Shaffer[b,c], and Yasu S. Morita[a,2]

a. Department of Microbiology, University of Massachusetts, Amherst, MA 01003, USA
b. Department of Biochemistry and Molecular Pharmacology, University of Massachusetts Medical School, Worcester, MA 01605 USA
c. Mass Spectrometry Facility, University of Massachusetts Medical School, Shrewsbury, MA 01545 USA

[1] These authors contributed equally to this work.
[2] To whom correspondence should be addressed. Department of Microbiology, University of Massachusetts, 639 North Pleasant Street, Amherst MA 01003, USA. Tel: +1-413-545-4604, Fax: +1-413-545-1578, E-mail: ymorita@microbio.umass.edu

Current addresses:
Julia Puffal, Department of Biochemistry and Molecular Biology, Rutgers University, NJ, USA.
Xuni Li, Sanofi Genzyme, Framingham, MA, USA.
Jennifer M. Hayashi, Gladstone Institute of Virology, San Francisco, CA, USA.

Running title:
Membrane domain in *Mycobacterium tuberculosis*

Keywords:
Cell envelope, cell membranes, glycolipids, lipid synthesis membrane proteins, *Mycobacterium tuberculosis*.

Abstract (250 words)

The intracellular membrane domain (IMD) is a metabolically active and laterally discrete membrane domain initially discovered in *Mycobacterium smegmatis*. The IMD correlates both temporally and spatially with the polar cell envelope elongation in *M. smegmatis*. Whether or not a similar membrane domain exists in pathogenic species remains unknown. Here we show that the IMD is a conserved membrane structure found in *Mycobacterium tuberculosis*. We used two independent approaches, density gradient fractionation of membrane domains and visualization of IMD-associated proteins through fluorescence microscopy, to determine the characteristics of the plasma membrane compartmentalization in *M. tuberculosis*. Proteomic analysis revealed that the IMD is enriched in metabolic enzymes that are involved in the synthesis of conserved cell envelope components such as peptidoglycan, arabinogalactan, and phosphatidylinositol mannosides. Using a fluorescent protein fusion of IMD-associated proteins, we demonstrated that this domain is concentrated in the polar region of the rod-shaped cells, where active cell envelope biosynthesis is taking place. Proteomic analysis further revealed the enrichment of enzymes involved in synthesis of phthiocerol dimycocerosates and phenolic glycolipids in the IMD. We validated the IMD association of two enzymes, α1,3-fucosyltransferase and fucosyl 4-*O*-methyltransferase, which are involved in the final maturation steps of phenolic glycolipid biosynthesis. Taken together, these data indicate that functional compartmentalization of membrane is an evolutionarily conserved feature found in both *M. tuberculosis* and *M. smegmatis*, and *M. tuberculosis* utilizes this membrane location for the synthesis of its surface-exposed lipid virulence factors.

51 **IMPORTANCE (150 words)**

52 *M. tuberculosis* remains an important public health threat, with more than one million deaths
53 every year. The pathogen's ability to survive in the human host for decades highlights the
54 importance of understanding how this bacterium regulates and coordinates its metabolism, cell
55 envelope elongation, and growth. The IMD is a membrane structure that associates with the
56 subpolar growth zone of actively growing mycobacteria, but its existence is only known in a non-
57 pathogenic model, *M. smegmatis*. Here, we demonstrated the presence of the IMD in *M.*
58 *tuberculosis*, making the IMD an evolutionarily conserved plasma membrane compartment in
59 mycobacteria. Furthermore, our study revealed that the IMD is the factory for synthesizing
60 phenolic glycolipids, virulence factors produced by slow-growing pathogenic species.

INTRODUCTION

Mycobacteria grow by depositing *de novo* synthesized cell envelope materials near the pole rather than the main sidewall of the rod-shaped cell (1–5). The cell envelope of mycobacteria is complex, composed of plasma membrane, peptidoglycan, arabinogalactan, and mycomembrane (6–9), making the spatially restricted cell envelope elongation a unique challenge for these bacteria. Precise coordination of the synthesis of cell envelope components are likely crucial, as highlighted by numerous proteins localizing to specific subcellular regions in mycobacteria (10). Among them, DivIVA, a filamentous coiled-coil protein, is associated with the pole of the cell and its physical interaction with early cell elongation machinery is implicated in the determination of the site of cell envelope elongation (11, 12). The recruitment of other enzymes involved in cell envelope biosynthesis defines a subpolar growth zone where new envelope components are made and incorporated into the growing pole (5, 11, 13). Polar enrichment is observed not only for proteins but also for membrane lipids. Plasma membrane heterogeneity was first reported using fluorescent lipid probes (14), and a more recent work suggested an enrichment of cardiolipin to the pole of growing mycobacterial cells (15).

Previously, we reported the presence of a growth-pole associated membrane domain, the intracellular membrane domain (IMD), in the nonpathogenic model organism *Mycobacterium smegmatis* (16–18). This domain is separated from the conventional plasma membrane upon density gradient fractionation of mycobacterial cell lysate. Plasma membrane is copurified with the cell wall, apparently due to physical connections between the two (termed PM-CW). The IMD, in contrast, is purified as ~50 nm membrane vesicles without the association of cell wall components. Among the proteins associated with the IMD, we find essential enzymes involved in lipid biosynthetic reactions. For instance, phosphatidylinositol mannosides (PIMs) are a major component of mycobacterial plasma membrane, and the initial phase of its biosynthesis is enriched in the IMD (16, 17). The IMD is not only present for cell envelope biosynthesis but also for other membrane-associated metabolisms. Menaquinone is a major respiratory chain electron carrier in mycobacteria, and the final maturation steps of its biosynthesis take place in the IMD (19). These observations indicate the diversity of crucial processes required for polar cell envelope growth and central metabolism that are associated with this membrane domain.

In *Mycobacterium tuberculosis*, we know comparatively less about subcellular localizations of membrane proteins. DivIVA is associated to the poles in *M. tuberculosis* (11) and CwsA, which

95 plays a role in cell wall synthesis and interacts with DivIVA, also shows polar and mid-cell
96 localization (20). On the other hand, FtsZ and its interacting partner SepF localize to future
97 division sites (21, 22). Furthermore, the sensor kinase MtrB localizes to septa in *M. tuberculosis*
98 as well (23). These past studies show conserved features of pole- and septum-associated
99 membrane proteins. However, other types of membrane compartmentalization have not been
100 reported in pathogenic mycobacteria. In this study, we investigated the presence of the IMD in
101 *M. tuberculosis*. Using subcellular fractionation, we first examined the IMD proteome in
102 comparison to the PM-CW proteome. We then visualized the localization of the IMD in live
103 growing *M. tuberculosis*. Our results demonstrate that the IMD is a membrane domain
104 conserved in mycobacteria.
105
106 **RESULTS**
107
108 **Density gradient fractionation of the *M. tuberculosis* cell lysate**
109 We prepared a lysate of exponentially growing *M. tuberculosis* cells and fractionated by density
110 gradient sedimentation (**Fig. 1A**). As previously seen in *M. smegmatis*, the majority of proteins
111 were enriched in the top two fractions. In the density gradient of *M. smegmatis* lysate,
112 cytoplasmic proteins are retained in the top fractions and do not sediment significantly. To
113 confirm that the *M. tuberculosis* proteins in the top fractions correspond to cytoplasmic proteins,
114 we performed immunoblotting against the cytoplasmic enzyme Ino1, an inositol-3-phosphate
115 synthetase (24), and detected this protein predominantly in fractions 1 - 2 (**Fig. 1B**). Next, we
116 determined the localization of the mannosyltransferase MptC, a polytopic membrane protein
117 found in the PM-CW in *M. smegmatis*, by immunoblotting. MptC was enriched in the denser
118 region of the gradient, spanning from fractions 8 - 11 (**Fig. 1B**). These fractions correspond to
119 the density of 1.127-1.154 g/ml, which is comparable to 1.131-1.159 g/ml for *M. smegmatis* PM-
120 CW (19), suggesting that MptC is a PM-CW protein in *M. tuberculosis* as well.
121
122 To examine if the IMD exists in *M. tuberculosis* in addition to the PM-CW fraction, we examined
123 the compositional profiles of plasma membrane phospholipids. Lipids were extracted from each
124 fraction and visualized by chemical staining. As shown in **Fig. 1C**, membrane phospholipids
125 cardiolipin (CL), phosphatidylethanolamine (PE), phosphatidylinositol (PI) and PIMs were
126 detected in the PM-CW fractions as well as in another density region spanning from fractions 3
127 to 6. These data suggest that there is an additional membrane fraction separate from the PM-
128 CW. One known reaction that takes place in *M. smegmatis* IMD is the biosynthesis of

129 polyprenol-phosphate-mannose (PPM). We have previously shown that the PPM biosynthetic
130 activity is enriched in the IMD and the enzyme Ppm1 was found exclusively in the IMD in *M.*
131 *smegmatis* (16, 17). To determine the localization of this biosynthetic reaction in *M.*
132 *tuberculosis*, we performed a cell-free radiolabeling assay using GDP-[^{3}H]mannose as a
133 mannose donor. As shown previously (25–27), *M. smegmatis* produces heptapentenyl and
134 decapentenyl PPM species (**Fig. S1**). In contrast, *M. tuberculosis* does not produce
135 heptapentenyl polyprenols, and decapentenyl PPM is the major product (27–29). Although the
136 enzyme activity is not as robust as that of *M. smegmatis* enzyme, we detected the synthesis of
137 the expected decapentenyl PPM from *M. tuberculosis* cell lysate (**Fig. S1**), and was enriched in
138 fractions 3 - 5 of a sucrose density gradient (**Fig. 1D**), suggesting the subcellular localization of
139 PPM synthetase in these membrane fractions.
140
141 To compare the morphology of the membrane present in fractions 3 - 5 with that of the PM-CW,
142 we precipitated these membrane fractions by differential centrifugation and visualized by
143 negative staining electron microscopy (EM) (**Fig. 1E**). As in *M. smegmatis* (17), we observed
144 small vesicle-like structures in fractions 3 - 5, while the PM-CW fraction revealed larger
145 fragments of cells. Together, these data support that fractions 3 - 5 correspond to the IMD in *M.*
146 *tuberculosis* and its overall characteristics are similar to those of the *M. smegmatis* IMD.
147
148 **Identification of IMD-associated proteins in *M. tuberculosis***
149 To uncover the IMD proteome, we purified the membranes in both IMD and PM-CW fractions by
150 differential centrifugation and analyzed the trypsin digests of total proteins by liquid
151 chromatography-mass spectrometry (LC-MS) in biological triplicates. The comparative
152 proteomes of the two membranes were distinct with a total of 64 or 298 proteins enriched more
153 than 2-fold ($p < 0.05$) in the PM-CW or IMD, respectively (**Fig. 2A**, **Dataset S1**). PM-CW was
154 associated with enzymes with activities that are related to the typical functions of plasma
155 membrane (**Fig. 2B**). For example, we identified Esx5 type VII secretion system components
156 EccB5-E5 (Rv1782, Rv1783, Rv1795), trehalose monomycolate transporter MmpL3 (Rv0206c),
157 a subunit of the phosphate specific transport system, PstS1 (Rv0934), and NADH-quinone
158 oxidoreductase subunits NuoF and NuoG (Rv3150, Rv3151). The IMD, on the other hand, was
159 more restricted to enzymes involved in lipid metabolism (**Fig 2B**). For instance, we found
160 enzymes involved in the synthesis of polyprenol-linked galactan precursor for arabinogalactan
161 synthesis enriched in the IMD: the GlcNAc-diphospho-decaprenol L-rhamnosyltransferase
162 WbbL1 (Rv3265c), the Rha-GlcNAc-diphospho-decaprenol β1,4/1,5-

163 galactofuranosyltransferase GlfT1 (Rv3782) and the Gal*f*-Gal*f*-Rha-GlcNAc-diphospho-
164 decaprenol β1,5/1,6-galactofuranosyltransferase GlfT2 (Rv3808c). The PPM synthase Ppm1
165 (Rv2051c) and acyl-CoA dehydrogenases such as FadE24 (Rv3139), FadE23 (Rv3140), and
166 FadE10 (Rv0873) were also found in the IMD. From the total of 298 proteins identified in the
167 IMD through the comparative proteomics, 218 had *M. smegmatis* homologues. Of these, 101
168 have also been identified previously as enriched in the IMD in a comparative proteomics of *M.*
169 *smegmatis* IMD and PM-CW (**Dataset S1**) (16). These data are consistent with the idea that the
170 *M. tuberculosis* IMD is a metabolically active membrane domain with multiple functions shared
171 with that of *M. smegmatis* (see below for a more refined IMD proteome).
172
173 **Validation of IMD-associated proteins**
174 Among the IMD-associated proteins was the dihydroorotate dehydrogenase PyrD, which is
175 involved in pyrimidine biosynthesis and is dependent on a lipidic electron carrier, menaquinone,
176 for the redox reaction (30, 31). Because it is an IMD-associated protein in *M. smegmatis* (16),
177 we chose this protein for the validation of the *M. tuberculosis* IMD proteome. We cloned the
178 gene with a hemagglutinin (HA) epitope tag into an expression vector, integrated into the
179 bacteriophage L5 integration site of *M. tuberculosis* genome, and confirmed its expected
180 molecular weight of 42.1 kDa (**Fig. 3A**). We then fractionated the cell lysate by sucrose density
181 gradient (**Fig. 3B**), and confirmed the IMD localization of PyrD-HA in contrast to the PM-CW
182 localization of MptC (**Fig. 3C**). These data indicate that PyrD associates with the IMD in *M.*
183 *tuberculosis* validating the comparative proteomics analysis.
184
185 Next, we took advantage of the PyrD-HA-expressing strain and purified the IMD from the
186 gradient fractions by vesicle immunoprecipitation using anti-HA agarose beads as performed
187 previously in *M. smegmatis* (16). We used the IMD fraction from the parental strain as a
188 negative control for immunoprecipitation. With a cutoff of 5-fold enrichment between the
189 experimental and negative control samples, 215 proteins were identified in the IMD of *M.*
190 *tuberculosis* (**Dataset S1**). Among them, 108 proteins were found in the IMD proteome of the
191 initial comparative proteomics (**Fig. 3D**). Out of these 215 immunoprecipitated proteins, 148 had
192 *M. smegmatis* homologues, with 73 localizing in the IMD of both species (**Fig. 3D**). Sixty seven
193 IMD-associated proteins were unique to *M. tuberculosis*, and notable proteins among them were
194 enzymes involved in the biosynthesis of phthiocerol dimycocerosate (PDIM) and phenolic
195 glycolipids (PGL; see below for further analysis). These data indicate that the IMD is an
196 evolutionarily conserved domain in mycobacteria with species-specific features.

197

198 **Visualization of IMD proteins in *M. tuberculosis***

199 To visualize the IMD in *M. tuberculosis*, we constructed a mutant, in which a gene encoding
200 2xHA-tagRFP tag was knocked into the 3' end of the endogenous *pyrD* gene locus. The in-
201 frame insertion was designed to produce a PyrD-2xHA-tagRFP fusion protein from the
202 endogenous locus using the native promoter. This mutant was grown to log phase, and cell
203 lysate was fractionated by sucrose density gradient. We detected the localization of this fusion
204 protein to the IMD by western blotting using anti-HA antibody (**Fig. 4**). When we examined this
205 strain by live fluorescence microscopy, we could not detect the fluorescence (not shown),
206 possibly due to low abundance of the protein expressed from the endogenous promoter.

207

208 As an alternative approach, we next used an expression vector that integrates at the
209 mycobacteriophage L5 *attB* site and expressed an IMD-associated protein as fluorescent
210 protein fusions using a strong promoter. We chose two proteins: GlfT2, a galactosyltransferase
211 involved in galactan biosynthesis, and Psd, a phosphatidylserine decarboxylase involved in PE
212 biosynthesis (see **Fig. 2A**). These enzymes are also enriched in the IMD of *M. smegmatis* (16,
213 17). We fractionated the lysates of cells expressing either GlfT2-mNeonGreen-HA or Psd-
214 mNeonGreen-HA. Both GlfT2-mNeonGreen-HA and Psd-mNeonGreen-HA showed expected
215 molecular weights (100.9 and 53.5 kDa, respectively), and were enriched in the IMD fractions
216 (**Fig. 5A-B and S2A-B**) although we noted that there was a weak signal of Psd-mNeonGreen-
217 HA in the PM-CW.

218

219 We then analyzed the localization of these proteins in live cells by fluorescence microscopy. In a
220 subset of cells, GlfT2-mNeonGreen-HA showed intense fluorescence near the poles of the cells
221 with less intense patches of fluorescence along the sidewall membrane (**Fig. 5C**). This
222 fluorescence pattern is consistent with the IMD fluorescence patterns observed in *M.*
223 *smegmatis*. We used structured illumination microscopy (SIM) to acquire higher-resolution
224 images. As shown in **Fig. 5D**, intense foci near the poles of the cells were evident and the
225 sidewall patches appeared consistent with the idea that the protein is a membrane-associated
226 protein. Even though the polar enrichment of GlfT2-mNeonGreen-HA was evident in some cells,
227 we often found many cells where the intensities of polar and sidewall patches were similar,
228 making the polar enrichment not as obvious as in the case of *M. smegmatis*. We considered the
229 possibility that the polar IMD enrichment may correlate with a specific cell cycle stage. To
230 visualize cells with or without an active septum synthesis, we labeled the cells with 3-[[(7-

231 hydroxy-2-oxo-2H-1-benzopyran-3-yl)carbonyl]amino]-D-alanine (HADA), a fluorescent D-amino
232 acid analog (**Fig. 5E**), and separated the cell population based on the presence of a septum.
233 We then determined the average fluorescence intensity profiles of GlfT2-mNeonGreen-HA
234 along the cell length as we have previously done in *M. smegmatis* (32). We observed that the
235 enrichment of GlfT2-mNeonGreen-HA was slightly proximal to the polar HADA labeling, and
236 was evident regardless of whether there is an active septum synthesis or not (**Fig. 5F**).
237 Comparable fluorescence patterns were also observed for Psd-mNeonGreen-HA (**Fig. S2C**).
238 Together, these data show that the IMD is a membrane domain that is frequently enriched in the
239 subpolar region of the cell.
240
241 **Maturation of PGL takes place in the IMD**
242 The biosynthesis pathways of PDIM and PGL are partially overlapping, utilizing the same
243 enzymes for several steps (**Fig. 6A**). The pathway can be divided into synthesis, assembly, and
244 maturation stages. In the synthesis stage, mycocerosates and (phenol)phthiocerols are
245 synthesized by Mas and PpsA-E, respectively. In the assembly stage, PapA5 esterifies two
246 molecules of mycocerosates to the hydroxyl groups of phthiocerol or phenolphthiocerol,
247 producing PDIM or a PGL precursor, phenolphthiocerol dimycocerosate (PPDIM), respectively.
248 In the maturation stage, PPDIM is further decorated at the hydroxyl group of the phenol residue
249 by several carbohydrate residues and these carbohydrates are modified by methylation to
250 become a mature PGL.
251
252 We found several enzymes in these pathways enriched in the IMD (**Fig. 6A**). Among them, we
253 generated merodiploid strains producing HA epitope-tagged PpsB, PpsE, and fPKR (Rv2951c).
254 PpsB and PpsE are polyketide synthases involved in the synthesis of (phenol)phthiocerols while
255 fPKR is a $F_{420}H_2$-dependent phthiodiolone ketoreductase (33–35). PpsE and fPKR were
256 enriched in the IMD based on the comparative analysis of IMD / PM-CW proteomes as well as
257 the proteome of immunoprecipitated IMD. PpsB was not found in the comparative proteome, but
258 identified in the immunoprecipitated IMD. We analyzed lysates of the merodiploid strains by
259 SDS-PAGE and anti-HA immunoblot, but were unable to detect any of these epitope-tagged
260 proteins (not shown). Next, we generated merodiploid strains producing mNeonGreen-HA-
261 tagged enzymes involved in the final maturation steps of PGL synthesis, namely a rhamnosyl *O*-
262 methyltransferase (Rv2959c), a fucosyltransferase (Rv2957), and a fucosyl *O*-methyltransferase
263 (Rv2955c). All three enzymes were enriched in the immunoprecipitated IMD. Rv2955c and
264 Rv2959c were also enriched in the IMD based on the IMD / PM-CW comparison. When

265 mNeonGreen-HA-tagged proteins were analyzed by immunoblot, we found significant amounts
266 of protein bands that were smaller than the expected molecular weight (not shown). We suspect
267 that those fluorescent protein-tagged fusions may be prone to protein degradation. To
268 circumvent the problem, we generated merodiploid strains producing fusion proteins tagged with
269 a short HA epitope alone. Among them, we detected a protein band that migrated near the
270 expected molecular weight for Rv2955c and Rv2957 whereas we could not detect Rv2959c at a
271 significant level. We fractionated a cell lysate from the strain producing either Rv2955c-HA or
272 Rv2957-HA, and determined the subcellular localization. Both proteins were localized to the
273 IMD although Rv2955c was distributing more broadly to a lighter density region as well (**Fig. 6B**
274 **and C**). Thus, our biochemical analysis validates that the final maturation steps of PGL
275 synthesis takes place in the IMD. Taken together with proteomic identifications, out data support
276 the idea that the majority of enzymatic reactions to synthesize PDIM/PGL take place in the IMD.
277

278 **DISCUSSION**

279 The IMD is proposed to provide a membrane surface for the cell envelope biosynthesis and
280 growth of *M. smegmatis*, a non-pathogenic model *Mycobacterium* (16, 17). Here, we
281 demonstrated that a similar membrane organization exists in *M. tuberculosis*. Furthermore, our
282 data demonstrate that the biosynthesis of PGL, a virulence factor produced by a subset of
283 pathogenic mycobacteria (36–40), takes place in the IMD. We suggest that the IMD is an
284 evolutionary conserved subcellular organization in mycobacteria.
285

286 A number of metabolic reactions in the IMD are conserved between the two species. First,
287 GlfT2, a galactofuranosyltransferase involved in arabinogalactan synthesis, was found in the
288 IMD of both species. Two reactions preceding the GlfT2-driven galactose chain elongation are
289 mediated by the rhamnosyltransferase WbbL1 (Rv3265c) and the galactofuranosyltransferase
290 GlfT1 (Rv3782). Both WbbL1 and GlfT1 are enriched in the IMD proteome of *M. smegmatis* as
291 well as *M. tuberculosis*, indicating that galactan precursor biosynthesis is a conserved metabolic
292 function of the IMD. Second, polyprenol-phosphate-mannose biosynthesis is IMD-associated in
293 *M. smegmatis* and the enzyme Ppm1 is enriched in this membrane domain (16, 17). In *M.*
294 *tuberculosis*, we used radiolabeled GDP-mannose to show the enzyme activity of Ppm1 in the
295 IMD. Furthermore, we detected Ppm1 (Rv2051c) in the *M. tuberculosis* comparative IMD
296 proteome although we could not detect this protein from the immunoprecipitated IMD. In *M.*
297 *smegmatis*, the PPM synthase Ppm1 and the integral membrane protein Ppm2 are produced
298 separately, while they are produced as a single fused polypeptide in *M. tuberculosis* (41). The

299 larger and more hydrophobic nature of *M. tuberculosis* Ppm1 may have contributed to the
300 inefficient detection of this protein by proteomics. Third, PyrD, a menaquinone-dependent
301 dihydroorotate dehydrogenase involved in pyrimidine biosynthesis, is an IMD-associated protein
302 in *M. smegmatis* (16, 42), and our current study revealed it as an IMD protein in *M. tuberculosis*
303 as well. These pathways represent some of the well-characterized evolutionarily conserved
304 pathways enriched in the IMD. In total, our data showed that 69-73% of the IMD-associated *M.*
305 *tuberculosis* proteins had *M. smegmatis* orthologs, which was comparable to the two-species
306 overlap found in the whole genome, where 63-69% of *M. tuberculosis* protein-coding genes
307 have *M. smegmatis* orthologs (43, 44).
308
309 It is notable that the IMD is often where final maturation steps of lipid biosynthesis take place.
310 For example, the final step of PE biosynthesis is decarboxylation of phosphatidylserine
311 mediated by the IMD-associated enzyme Psd (17, 42). We confirmed in this study that Psd
312 (Rv0437c), which was expressed as a mNeonGreen-HA fusion protein, is an IMD-associated
313 protein by both subcellular fractionation and fluorescence microscopy. Similarly, during the
314 synthesis of an electron carrier menaquinone, demethylmenaquinone produced by the PM-CW
315 enzyme MenA is modified by the IMD-associated demethylmenaquinone methyltransferase
316 MenG and menaquinone reductase MenJ to become a mature form of menaquinone (19). We
317 identified both MenG (Rv0558) and MenJ (Rv0561c) in the proteome of immunoprecipitated *M.*
318 *tuberculosis* IMD, suggesting a conserved compartmentalization of these final two steps of
319 menaquinone biosynthesis in the pathogenic species. Finally, peptidoglycan precursor lipid I
320 matures into lipid II by a GlcNAc transfer reaction mediated by MurG, and MurG is a previously
321 established IMD protein in *M. smegmatis* (32). In *M. tuberculosis*, MurG (Rv2153c) showed four-
322 fold enrichment in the IMD compared to the PM-CW, although we could not detect MurG in the
323 immunoprecipitated IMD proteome. Observations of conserved IMD-associated lipid maturation
324 steps in multiple lipid biosynthetic pathways indicate the role of the IMD in lipid modifications.
325
326 In addition to these shared features, *M. tuberculosis* IMD revealed roles that are specific to
327 slow-growing pathogens and not found in *M. smegmatis*. In particular, we found multiple
328 enzymes associated with the PDIM/PGL biosynthesis (Fig. 6A). These lipids are not produced
329 by *M. smegmatis*, and genes encoding the biosynthetic enzymes are absent in its genome. We
330 found PpsA-E (Rv2931-2935), polyketide synthases that produce phthiodiolone and
331 phenolphthiodiolone, enriched in the IMD proteomes. They are large proteins, ranging 159 - 231
332 kDa, and therefore, we were initially concerned if the IMD enrichment of PpsA and PpsE over

333 the PM-CW might have been a consequence of these large proteins sedimenting further in a
334 density gradient than other average-sized proteins due to their large size. However, all five
335 enzymes were identified in the proteome of immunoprecipitated IMD but not from the mock
336 immunoprecipitation of a wildtype cell lysate. Therefore, our data suggest that these enzymes
337 are truly associated with the IMD. Unfortunately, our attempts to express epitope-tagged PpsB
338 and PpsE were unsuccessful, and validation of the subcellular localization of these enzymes
339 must await future studies. PapA5 transfers two mycocerosates to either a phthiodiolone or a
340 phenolphthiodiolone, producing phthiodiolone dimycocerosate or phenolphthiodiolone
341 dimycocerosate, respectively. These lipids are further modified by sequential reactions of
342 $F_{420}H_2$-dependent phthiodiolone ketoreductase (fPKR, Rv2951c) and
343 phthiotriol/phenolphthiotriol dimycocerosates methyltransferase (PMT, Rv2952) to become a
344 mature PDIM or phenolphthiocerol dimycocerosate (PPDIM), a precursor of PGL (34, 35, 45,
345 46). Comparative proteomic analysis showed that both fPKR and PMT are enriched in the IMD,
346 and fPKR was also detected in the immunoprecipitated IMD. We attempted to express fPKR
347 with C-terminal mNeonGreen-HA or HA tag, but could not detect the protein production by
348 immunoblotting. fPKR has a predicted molecular weight of 41.3 kDa, and has no predicted
349 transmembrane domains. Therefore, it is likely that fPKR peripherally associates with the IMD,
350 but further validations are needed.
351
352 Finally, we attempted to produce epitope-tagged glycosyltransferases and methyltransferases
353 that are involved in the maturation of PPDIM to PGL. Two methyltransferases (Rv2955c and
354 Rv2959c) and a fucosyltransferase (Rv2957) were found in the IMD proteomes. While we could
355 not detect stable production of epitope-tagged Rv2959c, we were able to produce Rv2955c and
356 Rv2957 with C-terminal HA tag. Both proteins were found enriched in the IMD and absent in the
357 PM-CW, confirming the proteomic analysis. Rv2955c was more widely distributed into lighter
358 density regions (Fractions 2-3), which is a feature observed for some *M. smegmatis* proteins as
359 well (*e.g.* MurG, ThiD) (32, 42). The biochemically validated IMD association of two enzymes
360 involved in the final maturation step of PGL synthesis, combined with other enzymes found in
361 the IMD proteome, indicate that the PDIM/PGL biosynthesis takes place in the IMD.
362
363 In sum, we conclude that the IMD is a conserved membrane domain of mycobacteria enriched
364 in lipid biosynthetic reactions.
365
366 **MATERIALS AND METHODS**

367

368 **Cell cultures**

369 *M. tuberculosis mc^{2}6230 ΔRD1/panCD* strain was used throughout this study. It was grown in
370 Middlebrook 7H9 broth or Middlebrook 7H10 agar supplemented with OADC (final
371 concentrations: 190 μM oleic acid, 0.5% (w/v) bovine serum albumin, 11.1 mM dextrose, 13.9
372 mM NaCl, 0.0004% (w/v) catalase), 0.05% Tween 80, and 50 μg/ml pantothenic acid. When
373 required, the medium was supplemented with 100 μg/ml hygromycin B (Wako), 20 μg/ml
374 kanamycin sulfate (MP Biochemicals), 50 μg/ml streptomycin, or 5% sucrose.

375 **Density gradient fractionation and protein analysis**

376 Log phase cells (OD_{600} = 0.5-1.0) were lysed and the lysate was fractionated by sucrose density
377 gradient as described previously (16). The protein concentration for each fraction was
378 determined by bicinchoninic acid (BCA) assay (Pierce). Sucrose density of each fraction was
379 determined by a refractometer (ATAGO). SDS-PAGE and western blotting of the sucrose
380 gradient fractionation were performed using equal volume of each fraction as described before
381 (16). Anti-MptC antibody was previously raised (47) and anti-HA antibody was purchased from
382 Sigma-Aldrich.

383

384 **Cell-free radiolabeling assay**

385 To determine PPM biosynthesis activities, sucrose density fractions were incubated with GDP-
386 [2-^{3}H]mannose (American Radiolabeled Chemicals, 20 Ci/mmol) as described before (17),
387 except that the time of incubation was extended to 1 hour. The lipids were extracted, purified,
388 and resolved on high-performance thin layer chromatography (HPTLC) silica gel using
389 chloroform/methanol/13 M ammonia/1 M ammonium acetate/water (180:140:9:9:23, v/v/v/v/v)
390 as a solvent, and visualized by fluorography using En^{3}Hance.

391

392 **Lipid analysis**

393 Lipids were extracted from each gradient fraction as described (16) and analyzed by HPTLC as
394 described above. Phospholipids and PIMs were detected by molybdenum blue and orcinol
395 staining, respectively.

396

397 **Negative staining EM**

398 Samples of pooled sucrose gradient fractions of IMD and PM-CW were pelleted at 100,000x *g*
399 for 60 min on TLA100.2 rotor (Beckman), and washed with HES buffer (25mM HEPES-HCl, pH

400 7.4, 2mM EGTA, 150mM NaCl) twice. The samples were prepared for EM observation as
401 described (16).
402
403 **Proteome preparation and analysis**
404 Pooled IMD and PM-CW fractions were pelleted and washed, as described above, in biological
405 triplicates. The protein samples were then separated on a 12% SDS-PAGE gel for a short
406 distance and the gel slice containing the entire protein bands was subjected to in-gel trypsin
407 digestion. The peptides were analyzed by nano-LC ESI MS on an Orbitrap mass spectrometer
408 (Thermo Scientific Q Exactive) as described (16). The data were analyzed and annotated using
409 TubercuList (Release 27, https://mycobrowser.epfl.ch/). Proteins with a minimum of two-fold
410 enrichment ($p < 0.05$) in either the IMD or the PM-CW were considered to be part of the
411 respective proteome. Functional annotation was performed using DAVID Bioinformatics
412 Resources as described (16).
413
414 The immunoprecipitated IMD proteome was analyzed using IMD fractions from cells expressing
415 PyrD-HA, using wild-type as a negative control. Immunoprecipitation using HA-agarose beads
416 (Pierce), proteome analysis and functional annotation analysis were as described (16).
417
418 **Construction of plasmids**
419 pMUM036 – To create an expression vector for PyrD (Rv2139), which is C-terminally tagged
420 with an HA epitope, the *pyrD* gene was amplified with primers A161/A162 from *M. tuberculosis*
421 genomic DNA (**Table S1**). pMUM012 (16) was digested with EcoRV and ScaI and the vector
422 backbone was blunt-end-ligated with the PCR product.
423
424 pMUM145 – To create a knock-in strain, in which an epitope-tagged PyrD is expressed from the
425 endogenous locus, the upstream and downstream of the *pyrD* gene were amplified using
426 primers A536/A537 and A538/A539, respectively (**Table S1**). The PCR products were digested
427 with Van91I. The two fragments were then ligated into Van91I-digested pCOM1 as previously
428 described (16) to create an intermediate vector, pMUM133. Using pMV261-CO-TagRFP as a
429 template, tagRFP was amplified and HA tag was added using primers A557/A558. The PCR
430 product and pMUM133 were then digested with VspI and BspT1 and ligated to create a knock-in
431 vector to insert a gene encoding 2xHA-tagRFP at the 3' end of the *pyrD* gene.
432

433 pMUM215 – To create expression vector for C-terminally mNeonGreen-HA-tagged Psd
434 (Rv0437c), *psd* was cloned by PCR using primers A630/A631 (**Table S1**). In a separate
435 experiment, a gene encoding mNeonGreen was amplified from pMUM044, an unpublished
436 plasmid which carries the same *mNeonGreen* gene as our published plasmid pMUM072 (16),
437 using primers A483/A484. The PCR product was blunt-end-ligated with ScaI-digested
438 pMUM098 (19) to create pMUM111. The PCR product carrying *psd* and pMUM111 were
439 digested with NdeI and BspTI and ligated to create the final expression vector.
440
441 pMUM222 – To create an expression vector for GlfT2 (Rv3808c) with C-terminal mNeonGreen-
442 HA epitope tag, the *glfT2* gene was amplified with primers A628/A629 (**Table S1**). The PCR
443 product carrying *glfT2* and pMUM111 were digested with NdeI and BspTI and ligated to create
444 the final expression vector.
445
446 pMUM257 – We first created an expression vector for Rv2955c with C-terminal mNeonGreen-
447 HA epitope tag. The *rv2955c* gene was amplified with primers A849/850 (**Table S1**). Both the
448 PCR product carrying *rv2955c* and pMUM235, which is a derivative of pMUM111, were digested
449 with NdeI and BspTI and ligated to create the Rv2955c-mNeonGreen-HA expression vector
450 (pMUM245). To remove mNeonGreen, we digested pMUM245 with PacI and AflII, blunt-ended
451 the digested plasmid using T4 DNA polymerase, and ligated, resulting in pMUM257, the
452 Rv2955c-HA expression vector.
453
454 pMUM258 – As in pMUM257, we first created an expression vector for Rv2957 with C-terminal
455 mNeonGreen-HA epitope tag. The *rv2957* gene was amplified with primers A851/852 (**Table**
456 **S1**). The Rv2957-HA expression vector, pMUM246, and the Rv2957-HA expression vector,
457 pMUM258, were created following the identical procedure described for pMUM257.
458
459 Plasmid constructs were electroporated into *Mycobacterium tuberculosis* mc^2*6230*
460 *ΔRD1/panCD* for integration and homologous recombination as previously described (16).
461
462 **Fluorescence microscopy**
463 Standard fluorescence microscopy was performed as described (42). To distinguish between
464 cells with or without septa, cells were labeled with the peptidoglycan probe HADA (Tocris
465 Bioscience, Bristol, UK). *M. tuberculosis* cells expressing GlfT2-mNeonGreen-HA were grown to
466 mid-log (OD_{600} = 0.5) and then labeled with 500 μM HADA for 2 hour. Labeled cells were

467 washed twice in PBS, spotted onto a 1% agar pad slide and covered with a glass coverslip
468 sealed to the slide with nail polish. Live cells were then imaged with a Nikon Eclipse E600 with a
469 100x objective lens. mNeonGreen fluorescence profiles along cell lengths were calculated with
470 Oufti (48) and sorted based on the presence or absence of HADA-labelled septa. mNeonGreen
471 fluorescence profiles of septated and non-septated populations were aligned by their brightest
472 pole, normalized by cell length and then averaged using a custom Python script. For SIM,
473 images were acquired by Nikon Eclipse Ti N-SIM E microscope equipped with a Hamamatsu
474 Orca Flash 4.0 camera (numerical aperture,1.49) as described before (12), and reconstructed
475 on NIS Elements imaging software.
476

477 **Acknowledgement**

478 *M. tuberculosis mc^{2}6230 ΔRD1/panCD* strain, anti-Ino1 antibody, and pMV261-CO-TagRFP
479 plasmid were kind gifts from Drs. William Jacobs (Albert Einstein College of Medicine), Heran
480 Darwin (New York University), and Christopher Sassetti (University of Massachusetts Medical
481 School), respectively. Structured illumination super-resolution microscopy images were obtained
482 at the University of Massachusetts Light Microcopy Facility (Dr. James Chambers, Director),
483 with support from the Institute for Applied Life Sciences. This work was supported by NIH R03
484 AI140259 to YSM. JP was a recipient of the Science Without Borders Fellowship from CAPES-
485 Brazil (0328-13-8).
486

487 **REFERENCES**

488 1. Kieser KJ, Rubin EJ. 2014. How sisters grow apart: mycobacterial growth and division. Nat
489 Rev Microbiol 12:550–562.
490 2. Dulberger CL, Rubin EJ, Boutte CC. 2020. The mycobacterial cell envelope - a moving
491 target. Nat Rev Microbiol 18:47–59.
492 3. Aldridge BB, Fernandez-Suarez M, Heller D, Ambravaneswaran V, Irimia D, Toner M,
493 Fortune SM. 2012. Asymmetry and aging of mycobacterial cells lead to variable growth
494 and antibiotic susceptibility. Science 335:100–104.
495 4. Rego EH, Audette RE, Rubin EJ. 2017. Deletion of a mycobacterial divisome factor
496 collapses single-cell phenotypic heterogeneity. Nature 546:153–157.
497 5. García-Heredia A, Pohane AA, Melzer ES, Carr CR, Fiolek TJ, Rundell SR, Chuin Lim H,
498 Wagner JC, Morita YS, Swarts BM, Siegrist MS. 2018. Peptidoglycan precursor synthesis
499 along the sidewall of pole-growing mycobacteria. eLife 7:e37243.

500 6. Minnikin DE. 1982. Lipids: complex lipids, their chemistry biosynthesis and roles, p. 95–
501 184. *In* Ratledge, C, Stanford, J (eds.), The Biology of the Mycobacteria: Physiology,
502 Identification and Classification. Academic Press, London.
503 7. Rahlwes KC, Sparks IL, Morita YS. 2019. Cell walls and membranes of Actinobacteria.
504 Subcell Biochem 92:417–469.
505 8. Jankute M, Cox JAG, Harrison J, Besra GS. 2015. Assembly of the mycobacterial cell wall.
506 Annu Rev Microbiol 69:405–423.
507 9. Jackson M. 2014. The mycobacterial cell envelope-lipids. Cold Spring Harb Perspect Med
508 4:a021105–a021105.
509 10. Puffal J, García-Heredia A, Rahlwes KC, Siegrist MS, Morita YS. 2018. Spatial control of
510 cell envelope biosynthesis in mycobacteria. Pathog Dis 76:fty027.
511 11. Meniche X, Otten R, Siegrist MS, Baer CE, Murphy KC, Bertozzi CR, Sassetti CM. 2014.
512 Subpolar addition of new cell wall is directed by DivIVA in mycobacteria. Proc Natl Acad
513 Sci U S A 111:E3243-51.
514 12. Melzer ES, Sein CE, Chambers JJ, Siegrist MS. 2018. DivIVA concentrates mycobacterial
515 cell envelope assembly for initiation and stabilization of polar growth. Cytoskeleton
516 75:498–507.
517 13. Baranowski C, Welsh MA, Sham L-T, Eskandarian HA, Lim HC, Kieser KJ, Wagner JC,
518 McKinney JD, Fantner GE, Ioerger TR, Walker S, Bernhardt TG, Rubin EJ, Rego EH.
519 2018. Maturing *Mycobacterium smegmatis* peptidoglycan requires non-canonical
520 crosslinks to maintain shape. eLife 7:e37516.
521 14. Christensen H, Garton NJ, Horobin RW, Minnikin DE, Barer MR. 1999. Lipid domains of
522 mycobacteria studied with fluorescent molecular probes. Mol Microbiol 31:1561–1572.
523 15. Maloney E, Madiraju SC, Rajagopalan M, Madiraju M. 2011. Localization of acidic
524 phospholipid cardiolipin and DnaA in mycobacteria. Tuberc Edinb Scotl 91 Suppl 1:S150-
525 155.
526 16. Hayashi JM, Luo C-Y, Mayfield JA, Hsu T, Fukuda T, Walfield AL, Giffen SR, Leszyk JD,
527 Baer CE, Bennion OT, Madduri A, Shaffer SA, Aldridge BB, Sassetti CM, Sandler SJ,
528 Kinoshita T, Moody DB, Morita YS. 2016. Spatially distinct and metabolically active
529 membrane domain in mycobacteria. Proc Natl Acad Sci U S A 113:5400–5405.
530 17. Morita YS, Velasquez R, Taig E, Waller RF, Patterson JH, Tull D, Williams SJ, Billman-
531 Jacobe H, McConville MJ. 2005. Compartmentalization of lipid biosynthesis in
532 mycobacteria. J Biol Chem 280:21645–21652.

533 18. Hayashi JM, Richardson K, Melzer ES, Sandler SJ, Aldridge BB, Siegrist MS, Morita YS.
534 2018. Stress-induced reorganization of the mycobacterial membrane domain. mBio
535 9:e01823-17.
536 19. Puffal J, Mayfield JA, Moody DB, Morita YS. 2018. Demethylmenaquinone methyl
537 transferase is a membrane domain-associated protein essential for menaquinone
538 homeostasis in *Mycobacterium smegmatis*. Front Microbiol 9:3145.
539 20. Plocinski P, Arora N, Sarva K, Blaszczyk E, Qin H, Das N, Plocinska R, Ziolkiewicz M,
540 Dziadek J, Kiran M, Gorla P, Cross TA, Madiraju M, Rajagopalan M. 2012. *Mycobacterium*
541 *tuberculosis* CwsA interacts with CrgA and Wag31, and the CrgA-CwsA complex is
542 involved in peptidoglycan synthesis and cell shape determination. J Bacteriol 194:6398–
543 6409.
544 21. Gola S, Munder T, Casonato S, Manganelli R, Vicente M. 2015. The essential role of SepF
545 in mycobacterial division. Mol Microbiol 97:560–576.
546 22. Chauhan A, Madiraju MVVS, Fol M, Lofton H, Maloney E, Reynolds R, Rajagopalan M.
547 2006. *Mycobacterium tuberculosis* cells growing in macrophages are filamentous and
548 deficient in FtsZ rings. J Bacteriol 188:1856–1865.
549 23. Plocinska R, Purushotham G, Sarva K, Vadrevu IS, Pandeeti EVP, Arora N, Plocinski P,
550 Madiraju MV, Rajagopalan M. 2012. Septal localization of the *Mycobacterium tuberculosis*
551 MtrB sensor kinase promotes MtrA regulon expression. J Biol Chem 287:23887–23899.
552 24. Bachhawat N, Mande SC. 1999. Identification of the INO1 gene of *Mycobacterium*
553 *tuberculosis* H37Rv reveals a novel class of inositol-1-phosphate synthase enzyme. J Mol
554 Biol 291:531–536.
555 25. Wolucka BA, de Hoffmann E. 1998. Isolation and characterization of the major form of
556 polyprenyl-phospho-mannose from *Mycobacterium smegmatis*. Glycobiology 8:955–962.
557 26. Takayama K, Schnoes HK, Semmler EJ. 1973. Characterization of the alkali-stable
558 mannophospholipids of *Mycobacterium smegmatis*. Biochim Biophys Acta 316:212–221.
559 27. Crick DC, Schulbach MC, Zink EE, Macchia M, Barontini S, Besra GS, Brennan PJ. 2000.
560 Polyprenyl phosphate biosynthesis in *Mycobacterium tuberculosis* and *Mycobacterium*
561 *smegmatis*. J Bacteriol 182:5771–5778.
562 28. Takayama K, Goldman DS. 1970. Enzymatic synthesis of mannosyl-1-phosphoryl-
563 decaprenol by a cell-free system of *Mycobacterium tuberculosis*. J Biol Chem 245:6251–
564 6257.

565 29. Schulbach MC, Brennan PJ, Crick DC. 2000. Identification of a short (C_{15}) chain Z-
566 isoprenyl diphosphate synthase and a homologous long (C_{50}) chain isoprenyl diphosphate
567 synthase in *Mycobacterium tuberculosis*. J Biol Chem 275:22876–22881.
568 30. Björnberg O, Rowland P, Larsen S, Jensen KF. 1997. Active site of dihydroorotate
569 dehydrogenase A from *Lactococcus lactis* investigated by chemical modification and
570 mutagenesis. Biochemistry 36:16197–16205.
571 31. Munier-Lehmann H, Vidalain P-O, Tangy F, Janin YL. 2013. On dihydroorotate
572 dehydrogenases and their inhibitors and uses. J Med Chem 56:3148–3167.
573 32. García-Heredia A, Kado T, Sein CE, Puffal J, Osman SH, Judd J, Gray TA, Morita YS,
574 Siegrist MS. 2021. Membrane-partitioned cell wall synthesis in mycobacteria. eLife
575 10:e60263.
576 33. Onwueme KC, Vos CJ, Zurita J, Soll CE, Quadri LEN. 2005. Identification of phthiodiolone
577 ketoreductase, an enzyme required for production of mycobacterial diacyl phthiocerol
578 virulence factors. J Bacteriol 187:4760–4766.
579 34. Siméone R, Constant P, Malaga W, Guilhot C, Daffé M, Chalut C. 2007. Molecular
580 dissection of the biosynthetic relationship between phthiocerol and phthiodiolone
581 dimycocerosates and their critical role in the virulence and permeability of *Mycobacterium*
582 *tuberculosis*. FEBS J 274:1957–1969.
583 35. Purwantini E, Daniels L, Mukhopadhyay B. 2016. $F_{420}H_2$ is required for phthiocerol
584 dimycocerosate synthesis in mycobacteria. J Bacteriol 198:2020–2028.
585 36. Ng V, Zanazzi G, Timpl R, Talts JF, Salzer JL, Brennan PJ, Rambukkana A. 2000. Role of
586 the cell wall phenolic glycolipid-1 in the peripheral nerve predilection of *Mycobacterium*
587 *leprae*. Cell 103:511–524.
588 37. Tsenova L, Ellison E, Harbacheuski R, Moreira AL, Kurepina N, Reed MB, Mathema B,
589 Barry CE, Kaplan G. 2005. Virulence of selected *Mycobacterium tuberculosis* clinical
590 isolates in the rabbit model of meningitis is dependent on phenolic glycolipid produced by
591 the bacilli. J Infect Dis 192:98–106.
592 38. Sinsimer D, Huet G, Manca C, Tsenova L, Koo M-S, Kurepina N, Kana B, Mathema B,
593 Marras SAE, Kreiswirth BN, Guilhot C, Kaplan G. 2008. The phenolic glycolipid of
594 *Mycobacterium tuberculosis* differentially modulates the early host cytokine response but
595 does not in itself confer hypervirulence. Infect Immun 76:3027–3036.
596 39. Reed MB, Domenech P, Manca C, Su H, Barczak AK, Kreiswirth BN, Kaplan G, Barry CE.
597 2004. A glycolipid of hypervirulent tuberculosis strains that inhibits the innate immune
598 response. Nature 431:84–87.

599 40. Camacho LR, Ensergueix D, Perez E, Gicquel B, Guilhot C. 1999. Identification of a
600 virulence gene cluster of *Mycobacterium tuberculosis* by signature-tagged transposon
601 mutagenesis. Mol Microbiol 34:257–267.
602 41. Baulard AR, Gurcha SS, Engohang-Ndong J, Gouffi K, Locht C, Besra GS. 2003. *In vivo*
603 interaction between the polyprenol phosphate mannose synthase Ppm1 and the integral
604 membrane protein Ppm2 from *Mycobacterium smegmatis* revealed by a bacterial two-
605 hybrid system. J Biol Chem 278:2242–2248.
606 42. Rokicki CAZ, Brenner JR, Dills AH, Judd JJ, Kester JC, Puffal J, Sparks IL, Prithviraj M,
607 Anderson BR, Wade JT, Gray TA, Derbyshire KM, Fortune SM, Morita YS. 2021.
608 Fluorescence imaging-based discovery of membrane domain-associated proteins in
609 *Mycobacterium smegmatis*. J Bacteriol 203:e0041921.
610 43. Malhotra S, Vedithi SC, Blundell TL. 2017. Decoding the similarities and differences
611 among mycobacterial species. PLoS Negl Trop Dis 11:e0005883.
612 44. Namouchi A, Cimino M, Favre-Rochex S, Charles P, Gicquel B. 2017. Phenotypic and
613 genomic comparison of *Mycobacterium aurum* and surrogate model species to
614 *Mycobacterium tuberculosis*: implications for drug discovery. BMC Genomics 18:530.
615 45. Onwueme KC, Vos CJ, Zurita J, Soll CE, Quadri LEN. 2005. Identification of phthiodiolone
616 ketoreductase, an enzyme required for production of mycobacterial diacyl phthiocerol
617 virulence factors. J Bacteriol 187:4760–4766.
618 46. Pérez E, Constant P, Laval F, Lemassu A, Lanéelle M-A, Daffé M, Guilhot C. 2004.
619 Molecular dissection of the role of two methyltransferases in the biosynthesis of
620 phenolglycolipids and phthiocerol dimycoserosate in the *Mycobacterium tuberculosis*
621 complex. J Biol Chem 279:42584–42592.
622 47. Fukuda T, Matsumura T, Ato M, Hamasaki M, Nishiuchi Y, Murakami Y, Maeda Y,
623 Yoshimori T, Matsumoto S, Kobayashi K, Kinoshita T, Morita YS. 2013. Critical roles for
624 lipomannan and lipoarabinomannan in cell wall integrity of mycobacteria and pathogenesis
625 of tuberculosis. mBio 4:e00472-12.
626 48. Paintdakhi A, Parry B, Campos M, Irnov I, Elf J, Surovtsev I, Jacobs-Wagner C. 2016.
627 Oufti: an integrated software package for high-accuracy, high-throughput quantitative
628 microscopy analysis. Mol Microbiol 99:767–777.
629
630 **FIGURE LEGENDS**
631

632 **Figure 1**. Membrane compartmentalization in *M. tuberculosis* mc^{2}6230. **A**. Sucrose density
633 gradient fractionation of attenuated *M. tuberculosis* strain. The sucrose density and protein
634 concentration of the fractions are shown. **B**. Western blot detection of cytoplasmic marker Ino1
635 (40 kDa) and PM-CW marker MptC (47 kDa). **C**. Distribution of membrane phospholipids across
636 the gradient fractions. Phospholipids were stained by molybdenum blue staining. PIMs were
637 detected by orcinol staining. **D.** Cell-free PPM biosynthesis detection by GDP-[^{3}H]-Mannose
638 radiolabeling. **F.** Negative staining EM of the IMD and PM-CW fractions.
639
640 **Figure 2**. Comparative proteome of the conventional plasma membrane (PM-CW) and the IMD.
641 Cell growth, lysate preparation, membrane purification and proteomic analysis were repeated
642 three times. **A.** The volcano plot of proteins enriched in either the PM-CW or the IMD. Proteins
643 that were enriched more than two-fold with $p < 0.05$ were considered significant (black dots).
644 Other identified proteins are shown in gray dots. Red dots correspond to significantly enriched
645 proteins involved in PGL/PDIM biosynthesis. Green dots correspond to other proteins analyzed
646 biochemically and/or by fluorescent microscopy in this study. **B.** Functional annotation of
647 proteins enriched in the membrane fractions using UniProt keywords, showing that the IMD is
648 enriched in proteins related to membrane and lipid metabolism. The enrichment represents the
649 proportion of the term in the IMD proteome compared to its expected proportion in the genome.
650 The area of the circles are proportional to the number of proteins in each category.
651
652 **Figure 3**. PyrD is an IMD-associated protein. **A**. Western blotting of a crude lysate prepared
653 from a merodiploid *M. tuberculosis* strain producing PyrD-HA. In this strain, the expression
654 vector was integrated at L5 *attB* site. Expected molecular weight of PyrD-HA is 42.1 kDa. **B.**
655 Sucrose density gradient fractionation. The density and protein concentration for each fraction
656 are shown. **C**. Western blot detection of PyrD-HA in the IMD fractions and the PM-CW marker
657 MptC (Rv2181, 47 kDa). **D.** Proteome of an immunoprecipitated IMD. IMD was purified from the
658 PyrD-HA-expressing strain using anti-HA antibody. Left, Venn diagram showing the overlap of
659 proteins found in the comparative IMD proteome (Fig. 2) and immunoprecipitated IMD
660 proteome. Right, Venn diagram showing the orthologs found commonly in the
661 immunoprecipitated IMD proteomes of *M. tuberculosis* and *M. smegmatis*.
662
663 **Figure 4**. PyrD-2xHA-tagRFP, expressed from the endogenous locus, showing IMD
664 association. **A**. Sucrose gradient density fractionation of *M. tuberculosis* strain where the
665 endogenous *pyrD* gene was replaced with *pyrD-2xHA-tagRFP*. Sucrose density and protein

666 concentration for each fraction are shown. **B**. Western blot showing the IMD localization of
667 PyrD-2xHA-tagRFP (68.2 kDa). MptC, PM-CW marker (47 kDa). Experiments are repeated
668 twice and representative results are shown.
669
670 **Figure 5**. Polar enrichment and sidewall patches of GlfT2-mNeonGreen-HA, an IMD-associated
671 protein. **A.** Density gradient and protein concentration profile. **B.** Western blotting of GlfT2-
672 mNeonGreen-HA (100.9 kDa). MptC, PM-CW marker. **C.** Conventional fluorescence
673 microscopy images of log phase cells. **D.** SIM images of log phase cells. **E.** Cells expressing
674 GlfT2-mNeonGreen-HA, labeled with HADA for 2 hours and visualized by conventional
675 fluorescence microscopy. **F.** Fluorescence intensity profile of GlfT2-mNeonGreen-HA from cells
676 labeled with HADA, for which representative images are shown in the panel E. Cells were
677 categorized into two populations based on the presence or absence of a septum, as determined
678 by HADA labeling. Intensity profiles are aligned with the brightest pole on the left and are shown
679 in arbitrary units. Green and blue fluorescence intensity profiles correspond to GlfT2-
680 mNeonGreen-HA and HADA respectively. Experiments are repeated at least twice and
681 representative results are shown.
682
683 **Figure 6**. PDIM and PGL biosyntheses take place in the IMD. **A.** Biosynthetic pathways of
684 PDIM and PGL. Enzymes involved in the biosyntheses are shown in ovals, which are color-
685 coded to indicate the subcellular localization based on proteomic analyses. **B.** Western blotting
686 of Rv2955c-HA (37.8 kDa). **C.** Western blotting of Rv2957-HA (32.9 kDa). MptC, PM-CW
687 marker.
688
689 **Supplemental Figures**
690
691 **Figure S1**. Cell-free PPM biosynthesis detection of crude lysate by GDP-[^{3}H]-Mannose
692 radiolabeling, comparing *M. smegmatis* and *M. tuberculosis*.
693
694 **Figure S2**. IMD association of Psd-mNeonGreen-HA. **A.** Density gradient and protein
695 concentration profile. **B.** Western blotting of Psd-mNeonGreen-HA (53.5 kDa). MptC, PM-CW
696 marker. **C.** SIM images of log phase cells. Experiments are repeated twice and representative
697 results are shown.
698

699 **Table S1**. Primers to create plasmids used in this study.

700

Plasmid	Gene ID	Protein	Forward Primer Reverse Primer	
pMUM036	Rv2139	PyrD	A161	ATCCATATGTATCCCCTGGTGCGT
			A162	ACTGCTGGGTTGCCGACGTCTT
pMUM145	Upstream of Rv2139	PryD knock-in	A536	TTTTTTTTCCATAGATTGGCACAAGTTGGTTTTCGCCGTG
			A537	TTTTTTTTCCATATTTTGGATTAATGCTGGGTTGCCGACGTCTT
	TagRFP		A557	TTTTTTTTATTAATTACCCGTACGACGTCCCGGACTACGCGTACCC GTACGACGTCCCGGACTACGCGCAATTGAGCAAGGGCGAGGAGCTG
			A558	TTTTTTTTCTTAAGCTTGTAGAGCTCGTCCATGCC
	Downstream of Rv2139		A538	TTTTTTTTCCATAATTTGGCTTAAGTAAAGCGCTAACGCTGCTCG
			A539	TTTTTTTTCCATCTTTTGGATACAAGGCCAACGTCGTCC
pMUM215	mNeonGreen	Psd-mNeon Green	A483	ACTCTTAAGATGGTTAGTAAAAGAGAAGAAGA
			A484	ACTGTTAATTAACAATTGTTTGTAGAGCTCATCCATGCCA
	Rv0437c		A630	TTTTTTTTTCATATGGTGGCCAGACGCCCCCGC
			A631	TTTTTCTTAAGCAATTGTCGACATTCGGCCAGCACGG
pMUM222	Rv3808c	GlfT2	A628	TTTTTTTTTCATATGATGAGTGAACTCGCCGC
			A629	TTTTTCTTAAGCAATTGGCCATGCTCGGGCTCT
pMUM257	Rv2955c	Rv2955c	A849	TTTTTTTTCATATGCAGTTCCAAGATGTGCGCC
			A850	TTTTTTTTCTTAAGTCCCTTCCGGCTCGGAATAAAGA
pMUM258	Rv2957	Rv2957	A851	GTGGCAGAAAAGACGTCCGA
			A852	CACGTCGTAGTAGAGCGAGAACT

Figure 1

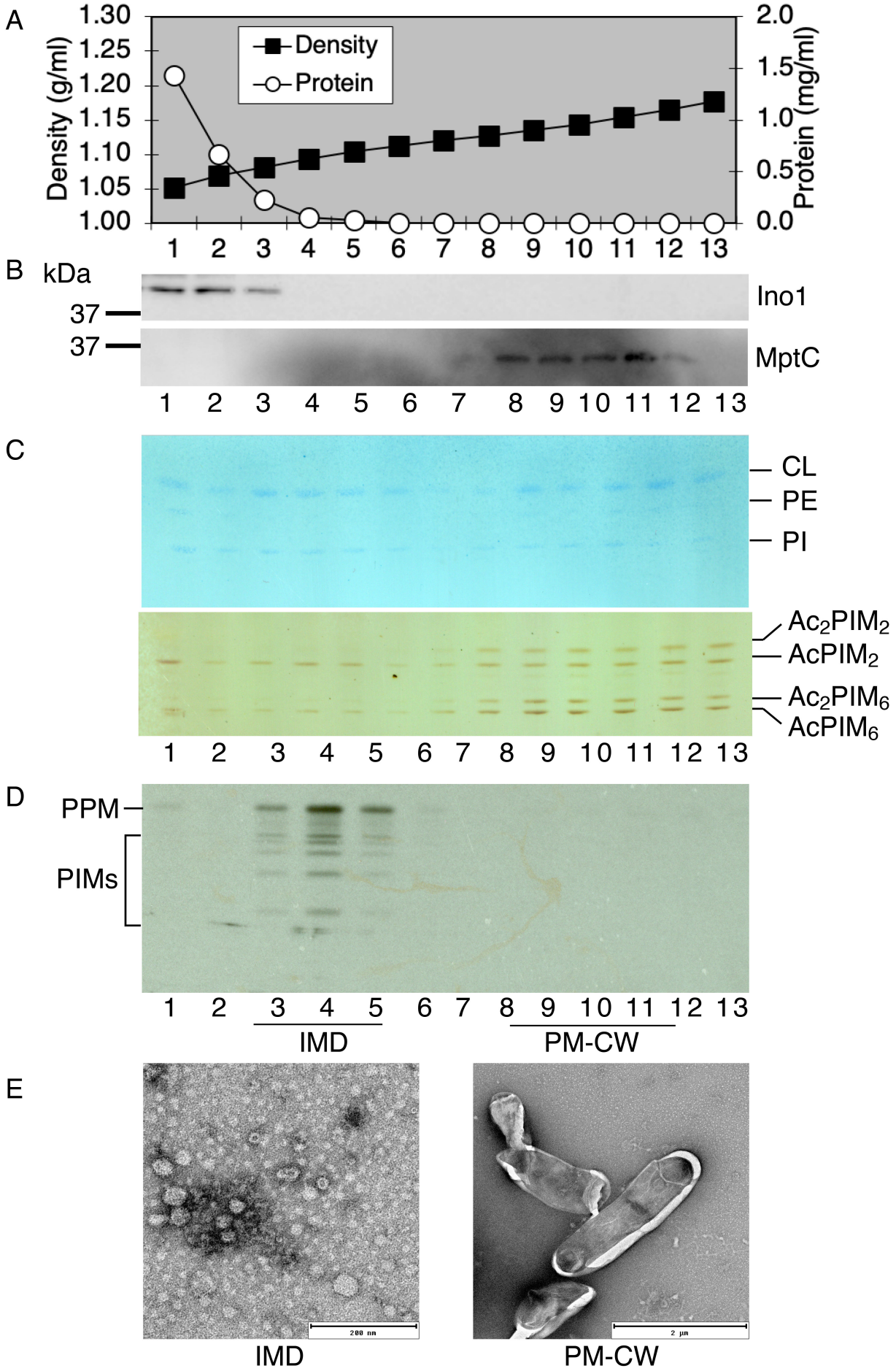
A
Density (g/ml)
1.30
1.25
1.20
1.15
1.10
1.05
1.00
Protein (mg/ml)
2.0
1.5
1.0
0.5
0.0
Density
Protein
1 2 3 4 5 6 7 8 9 10 11 12 13
B
kDa
37
37
Ino1
MptC
1 2 3 4 5 6 7 8 9 10 11 12 13
C
CL
PE
PI
Ac2PIM2
AcPIM2
Ac2PIM6
AcPIM6
1 2 3 4 5 6 7 8 9 10 11 12 13
D
PPM
PIMs
1 2 3 4 5 6 7 8 9 10 11 12 13
IMD
PM-CW
E
200 nm
2 µm
IMD
PM-CW

Figure 2

A

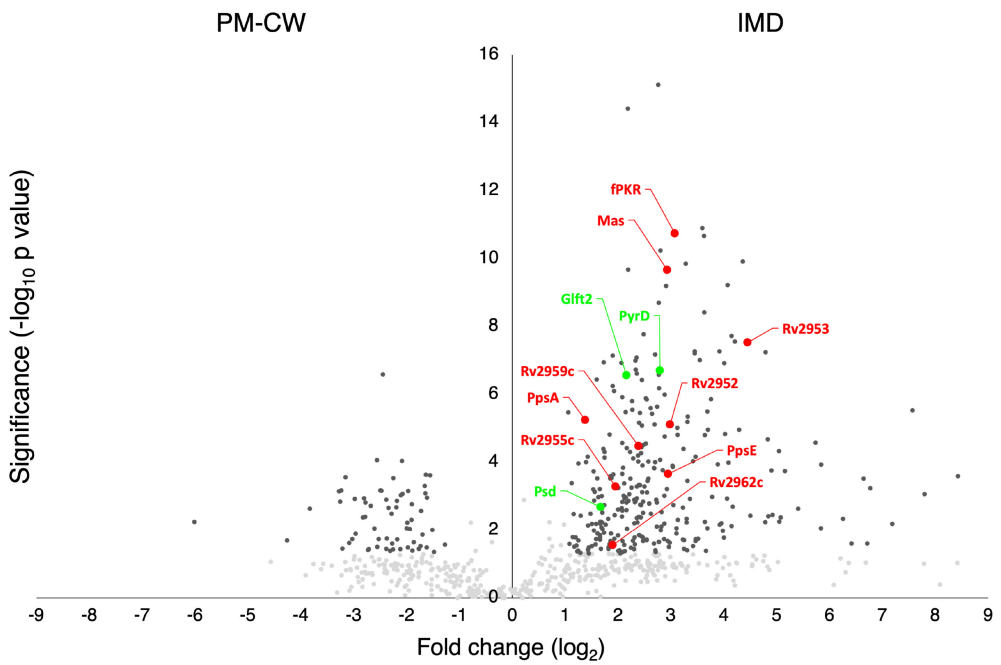
PM-CW
IMD
Significance (-log10 p value)
Fold change (log2)
fPKR
Mas
Glft2
PyrD
Rv2953
Rv2959c
Rv2952
PpsA
Rv2955c
PpsE
Rv2962c
Psd

B

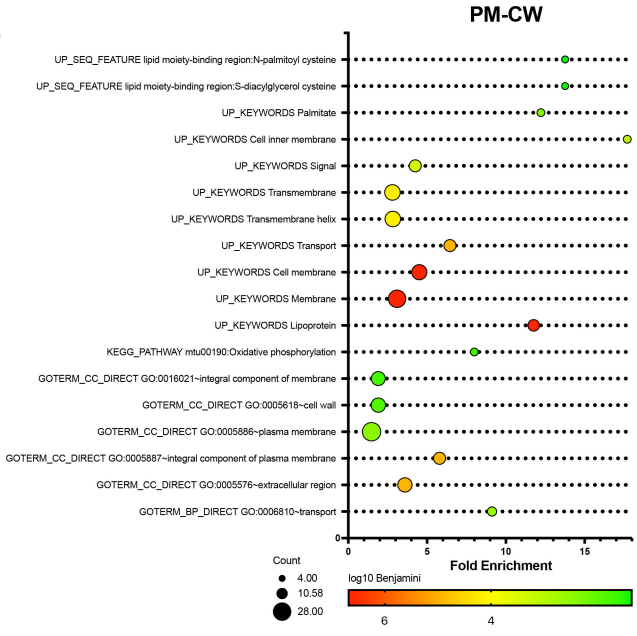
PM-CW
UP_SEQ_FEATURE lipid moiety-binding region:N-palmitoyl cysteine
UP_SEQ_FEATURE lipid moiety-binding region:S-diacylglycerol cysteine
UP_KEYWORDS Palmitate
UP_KEYWORDS Cell inner membrane
UP_KEYWORDS Signal
UP_KEYWORDS Transmembrane
UP_KEYWORDS Transmembrane helix
UP_KEYWORDS Transport
UP_KEYWORDS Cell membrane
UP_KEYWORDS Membrane
UP_KEYWORDS Lipoprotein
KEGG_PATHWAY mtu00190:Oxidative phosphorylation
GOTERM_CC_DIRECT GO:0016021~integral component of membrane
GOTERM_CC_DIRECT GO:0005618~cell wall
GOTERM_CC_DIRECT GO:0005886~plasma membrane
GOTERM_CC_DIRECT GO:0005887~integral component of plasma membrane
GOTERM_CC_DIRECT GO:0005576~extracellular region
GOTERM_BP_DIRECT GO:0006810~transport
Fold Enrichment
Count
4.00
10.58
28.00
log10 Benjamini
6
4

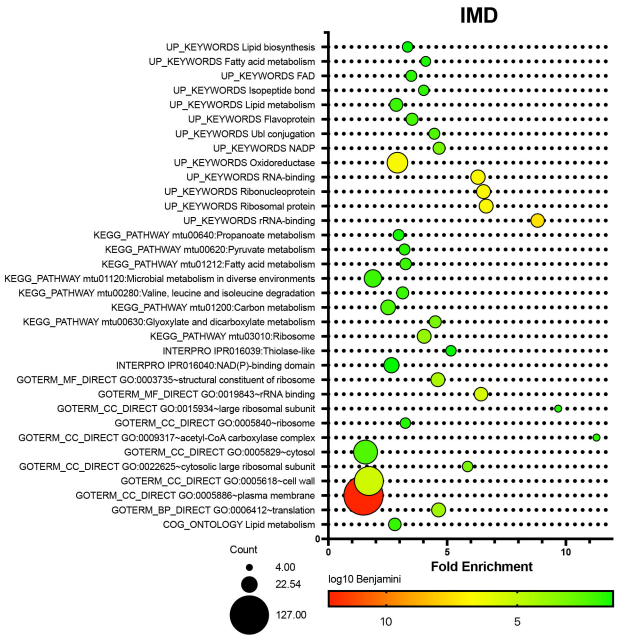
IMD
UP_KEYWORDS Lipid biosynthesis
UP_KEYWORDS Fatty acid metabolism
UP_KEYWORDS FAD
UP_KEYWORDS Isopeptide bond
UP_KEYWORDS Lipid metabolism
UP_KEYWORDS Flavoprotein
UP_KEYWORDS Ubl conjugation
UP_KEYWORDS NADP
UP_KEYWORDS Oxidoreductase
UP_KEYWORDS RNA-binding
UP_KEYWORDS Ribonucleoprotein
UP_KEYWORDS Ribosomal protein
UP_KEYWORDS rRNA-binding
KEGG_PATHWAY mtu00640:Propanoate metabolism
KEGG_PATHWAY mtu00620:Pyruvate metabolism
KEGG_PATHWAY mtu01212:Fatty acid metabolism
KEGG_PATHWAY mtu01120:Microbial metabolism in diverse environments
KEGG_PATHWAY mtu00280:Valine, leucine and isoleucine degradation
KEGG_PATHWAY mtu01200:Carbon metabolism
KEGG_PATHWAY mtu00630:Glyoxylate and dicarboxylate metabolism
KEGG_PATHWAY mtu03010:Ribosome
INTERPRO IPR016039:Thiolase-like
INTERPRO IPR016040:NAD(P)-binding domain
GOTERM_MF_DIRECT GO:0003735~structural constituent of ribosome
GOTERM_MF_DIRECT GO:0019843~rRNA binding
GOTERM_CC_DIRECT GO:0015934~large ribosomal subunit
GOTERM_CC_DIRECT GO:0005840~ribosome
GOTERM_CC_DIRECT GO:0009317~acetyl-CoA carboxylase complex
GOTERM_CC_DIRECT GO:0005829~cytosol
GOTERM_CC_DIRECT GO:0022625~cytosolic large ribosomal subunit
GOTERM_CC_DIRECT GO:0005618~cell wall
GOTERM_CC_DIRECT GO:0005886~plasma membrane
GOTERM_BP_DIRECT GO:0006412~translation
COG_ONTOLOGY Lipid metabolism
Fold Enrichment
Count
4.00
22.54
127.00
log10 Benjamini
10
5

Figure 3

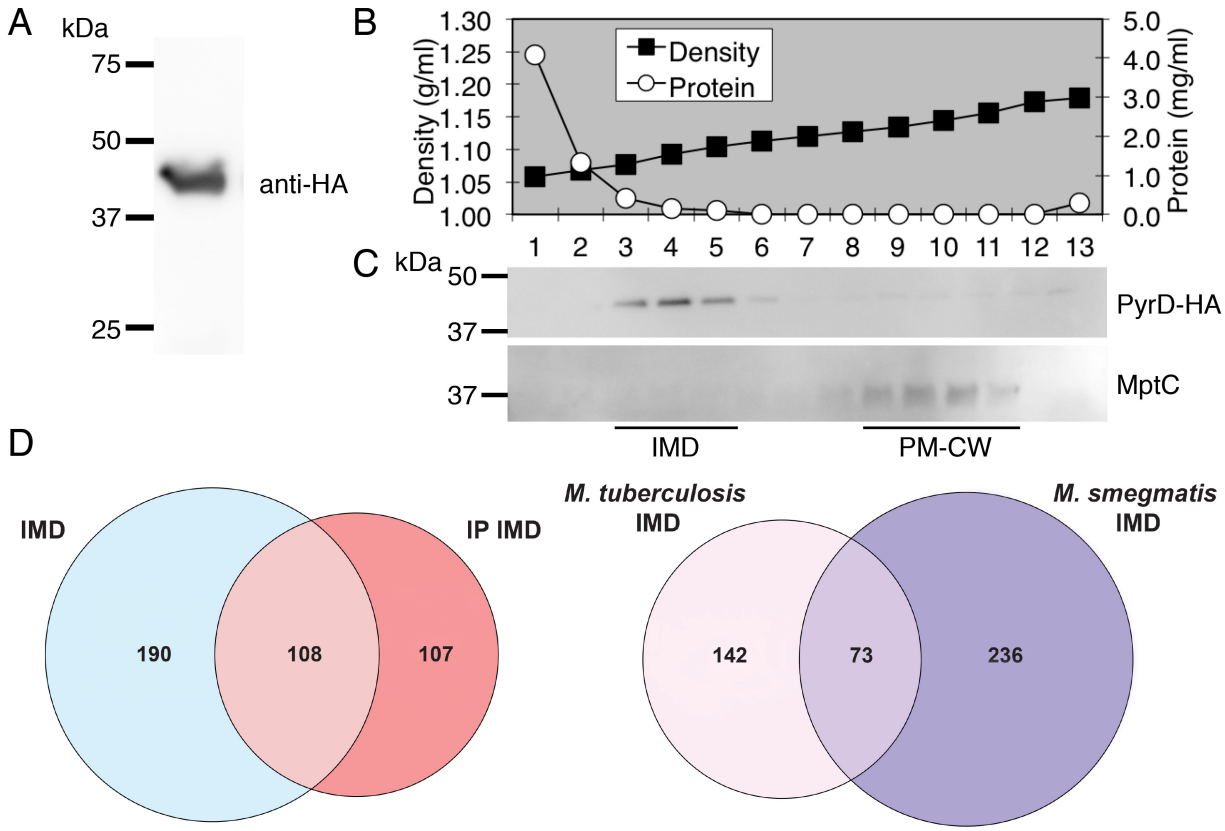
A
kDa
75
50
37
25
anti-HA
B
Density
Protein
Density (g/ml)
Protein (mg/ml)
1.30
1.25
1.20
1.15
1.10
1.05
1.00
5.0
4.0
3.0
2.0
1.0
0.0
1 2 3 4 5 6 7 8 9 10 11 12 13
C
kDa
50
37
PyrD-HA
37
MptC
IMD
PM-CW
D
IMD
IP IMD
190
108
107
M. tuberculosis
IMD
M. smegmatis
IMD
142
73
236

Figure 4

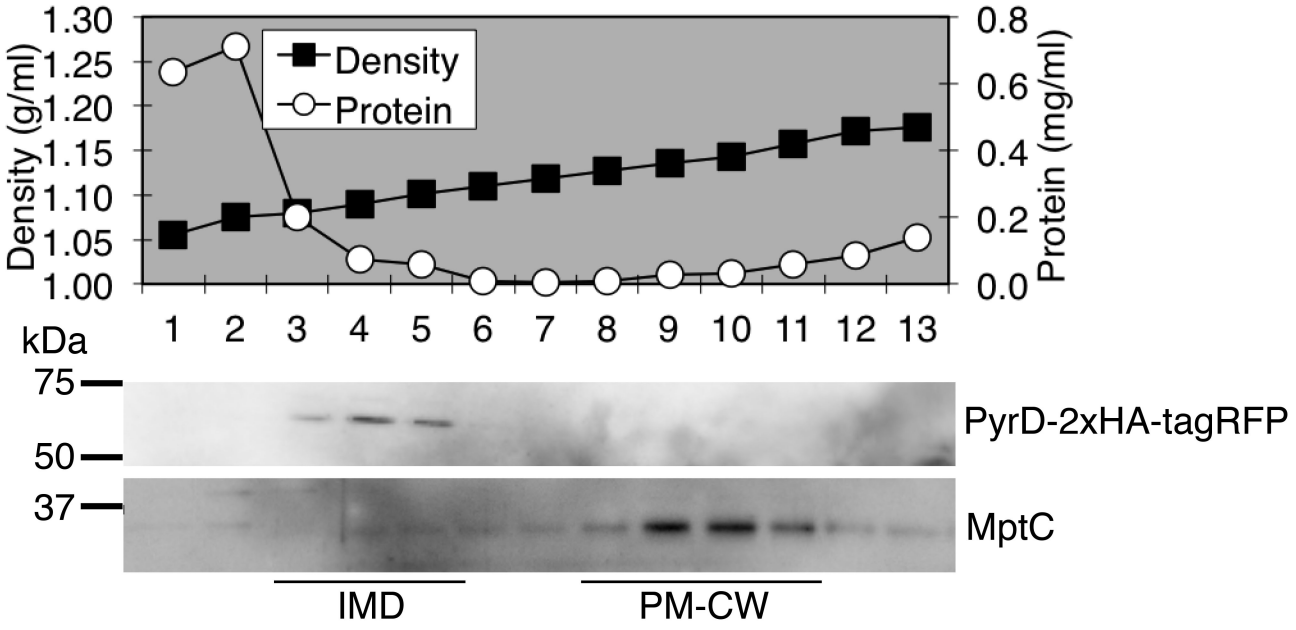
Density (g/ml)
1.30
1.25
1.20
1.15
1.10
1.05
1.00
Density
Protein
0.8
0.6
0.4
0.2
0.0
Protein (mg/ml)
1 2 3 4 5 6 7 8 9 10 11 12 13
kDa
75
50
37
PyrD-2xHA-tagRFP
MptC
IMD
PM-CW

Figure 5

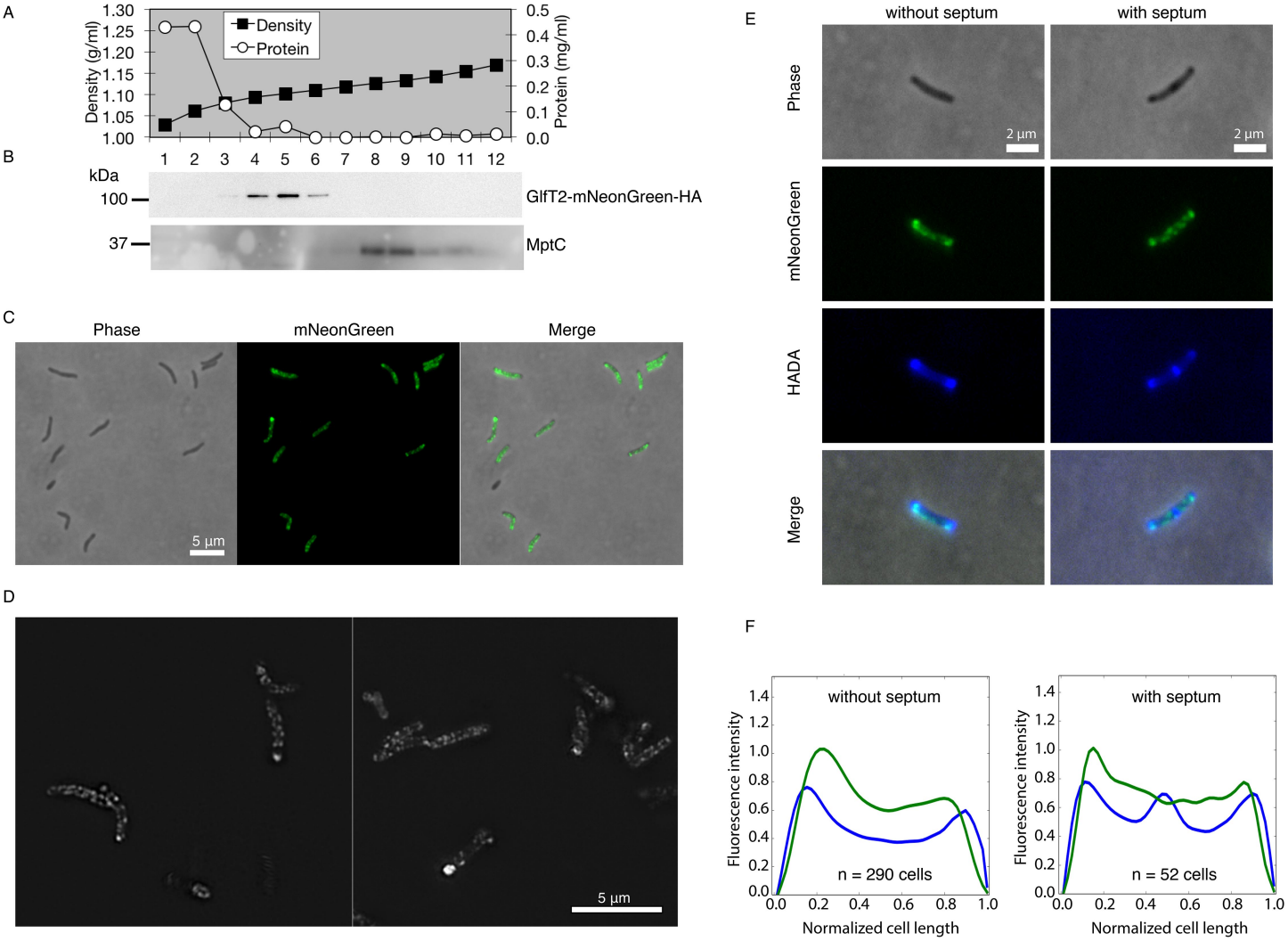
A
Density
Protein
Density (g/ml)
Protein (mg/ml)
1.30
1.25
1.20
1.15
1.10
1.05
1.00
0.5
0.4
0.3
0.2
0.1
0.0
1 2 3 4 5 6 7 8 9 10 11 12
B
kDa
100
37
GlfT2-mNeonGreen-HA
MptC
C
Phase
mNeonGreen
Merge
5 µm
D
5 µm
E
without septum
with septum
Phase
mNeonGreen
HADA
Merge
2 µm
2 µm
F
without septum
with septum
Fluorescence intensity
n = 290 cells
n = 52 cells
Normalized cell length
Normalized cell length

Fig. 6

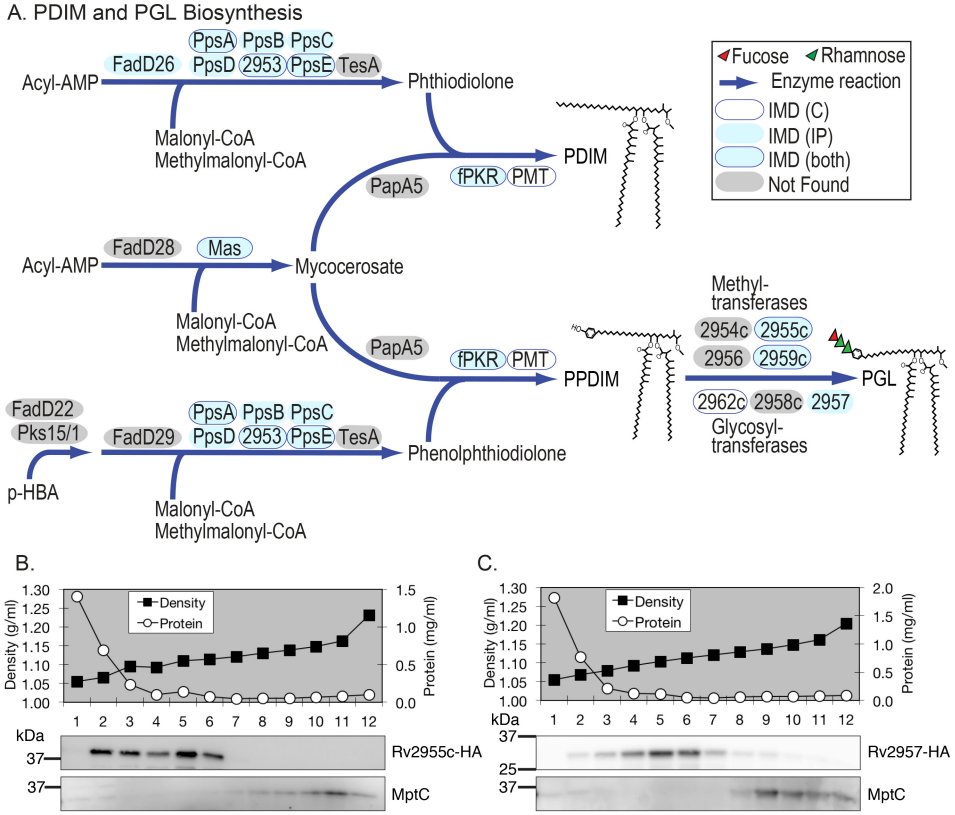
A. PDIM and PGL Biosynthesis
PpsA PpsB PpsC
FadD26 PpsD 2953 PpsE TesA
Acyl-AMP
Phthiodiolone
Malonyl-CoA
Methylmalonyl-CoA
PDIM
fPKR PMT
PapA5
Fucose
Rhamnose
Enzyme reaction
IMD (C)
IMD (IP)
IMD (both)
Not Found
FadD28 Mas
Acyl-AMP
Mycocerosate
Malonyl-CoA
Methylmalonyl-CoA
PapA5
fPKR PMT
PPDIM
Methyl-transferases
2954c 2955c
2956 2959c
2962c 2958c 2957
Glycosyl-transferases
PGL
FadD22
Pks15/1
p-HBA
PpsA PpsB PpsC
FadD29 PpsD 2953 PpsE TesA
Phenolphthiodiolone
Malonyl-CoA
Methylmalonyl-CoA
B.
Density
Protein
Density (g/ml)
Protein (mg/ml)
kDa
Rv2955c-HA
MptC
C.
Density
Protein
Density (g/ml)
Protein (mg/ml)
kDa
Rv2957-HA
MptC

Figure S1

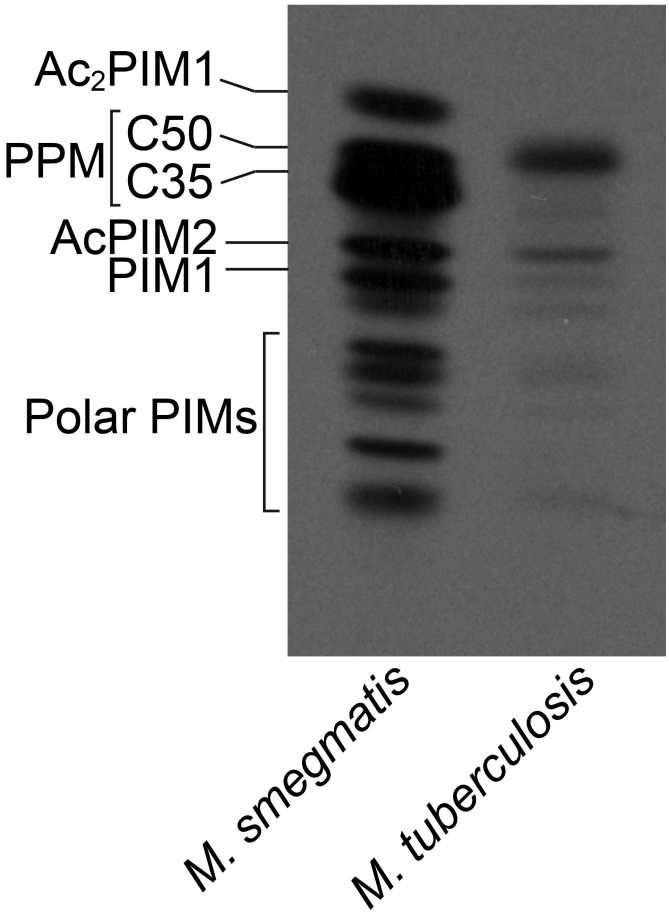
Ac2PIM1
PPM
C50
C35
AcPIM2
PIM1
Polar PIMs
M. smegmatis
M. tuberculosis

Figure S2

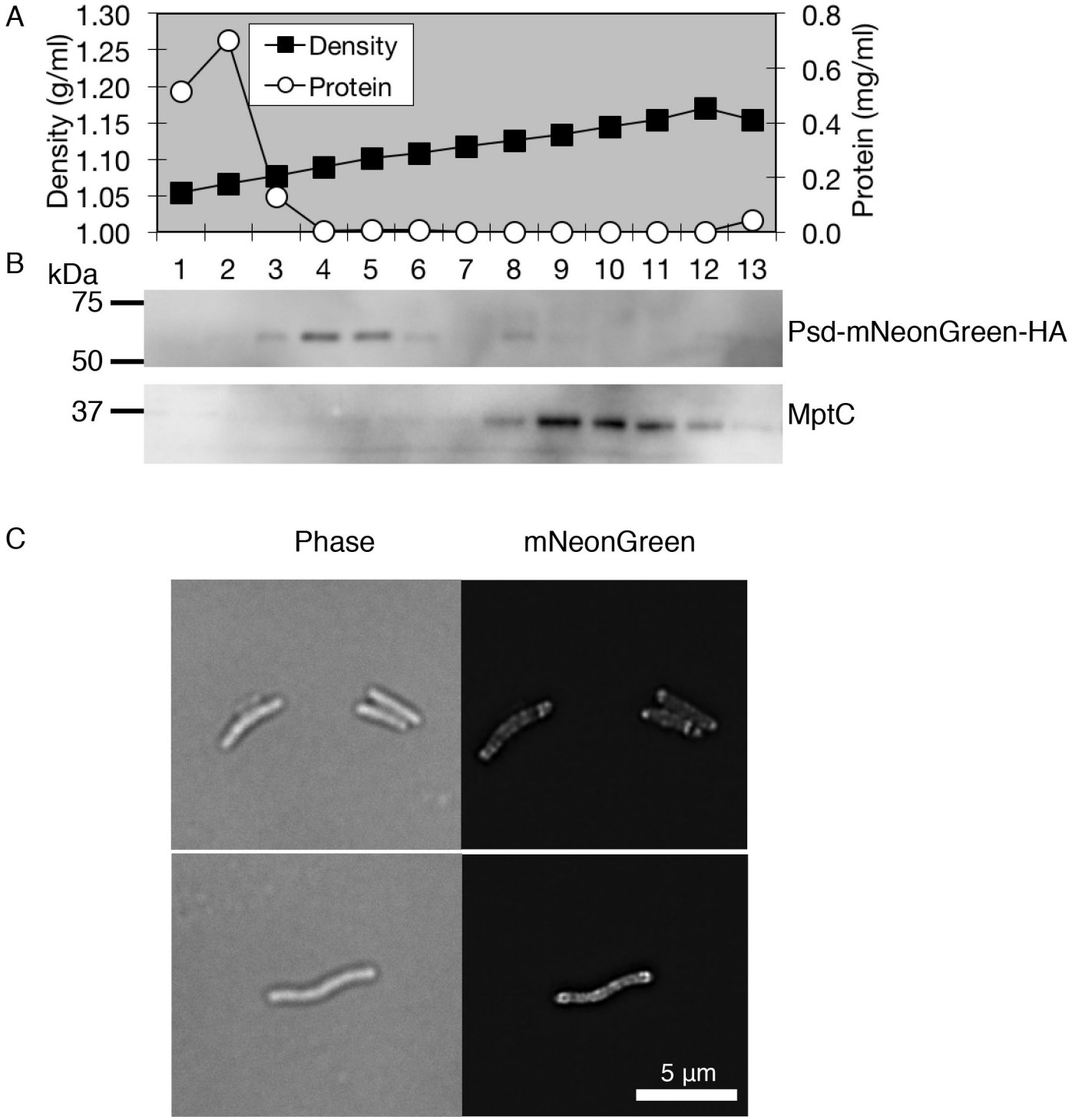
A
Density (g/ml)
1.30
1.25
1.20
1.15
1.10
1.05
1.00
Density
Protein
0.8
0.6
0.4
0.2
0.0
Protein (mg/ml)
B
kDa
1 2 3 4 5 6 7 8 9 10 11 12 13
75
50
37
Psd-mNeonGreen-HA
MptC
C
Phase
mNeonGreen
5 µm